ACS chemical biology

pubs.acs.org/acschemicalbiology

Articles

Base Pairing and Functional Insights into N^3-Methylcytidine (m^3C) in RNA

Song Mao, Phensinee Haruehanroengra, Srivathsan V. Ranganathan, Fusheng Shen, Thomas J. Begley, and Jia Sheng*

Cite This: *ACS Chem. Biol.* 2021, 16, 76–85

Read Online

ACCESS | Metrics & More | Article Recommendations | Supporting Information

ABSTRACT: N^3-methylcytidine (m^3C) is present in both eukaryotic tRNA and mRNA and plays critical roles in many biological processes. We report the synthesis of the m^3C phosphoramidite building block and its containing RNA oligonucleotides. The base-pairing stability and specificity studies show that the m^3C modification significantly disrupts the stability of the Watson−Crick C:G pair. Further m^3C decreases the base pairing discrimination between C:G and the other mismatched C:A, C:U, and C:C pairs. Our molecular dynamic simulation study further reveals the detailed structural insights into the m^3C:G base pairing pattern in an RNA duplex. More importantly, the biochemical investigation of m^3C using reverse transcription *in vitro* shows that N^3-methylation specifies the C:A pair and induces a G to A change using HIV-1-RT, MMLV-RT, and MutiScribe-RT enzymes, all with relatively low replication fidelity. For other reverse transcriptases with higher fidelity like AMV-RT, the methylation could completely shut down DNA synthesis. Our work provides detailed insights into the thermostability of m^3C in RNA and a foundation for developing new molecular tools for mapping m^3C in different RNA contexts and exploring the biochemical and biomedical potentials of m^3C in the design and development of RNA based therapeutics.

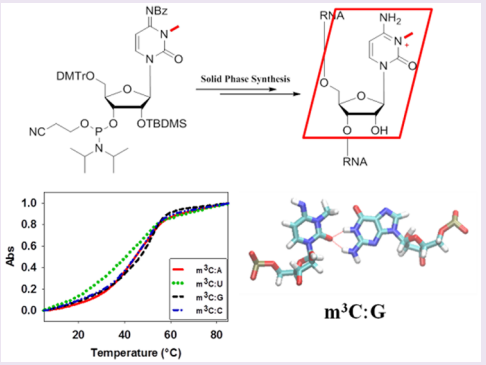

INTRODUCTION

Natural RNA systems in all organisms, from the simplest prokaryote *Nanoarchaeum equitans* to humans, utilize the four regular nucleosides (adenosine, guanosine, cytidine, and uridine) and a variety of post-transcriptional modifications to achieve structural and functional specificity and diversity.[1] To date, more than 160 distinct chemical modifications that decorate different positions of nucleobases, ribose, and the phosphate backbone in RNA nucleotides have been discovered,[2−6] since the first discovery of the modified nucleoside in the 1950s.[7,8] Many RNA modifications have been demonstrated to play critical roles in both normal and disease cellular functions and processes, such as development, circadian rhythms, embryonic stem cell differentiation, meiotic progression, temperature adaptation, stress response and tumorigenesis, etc.[4] Similar to DNA and protein based epigenetic markers, RNA modifications (also termed the "epitranscriptome") are dynamically and reversibly regulated by specific reader, writer, and eraser enzymes, representing a new layer of gene regulation.[9] Accordingly, RNA modification-associated enzymes, as an important research frontier toward RNA-based drug discovery, have become useful molecular tools and drug targets.[10]

Benefiting from a variety of recently developed chemical biology tools and high-throughput detection strategies, RNA methylation has been identified in different RNAs from all organisms.[9,11−16] In addition, corresponding writers and erasers and bonding proteins ("readers")[17] have been identified for many RNA methylations and shown to impact numerous biological functions and disease processes. For example, the tRNA methylations 5-methylcytidine (m^5C), N^1-methylguanidine (m^1G), N^1-methyladenosine (m^1A), N^7-methylguanidine (m^7G), and 2′-O-methylated sugar (2′-Nm) in the anticodon stem loops of transfer RNA (tRNA) are directly involved in the codon recognition and can induce or inhibit frameshifting mutations during translation.[18,19] In addition, N^6-methyladenosine (m^6A), the most abundant internal mRNA methylation, is linked to numerous biological functions, including mRNA stability, RNA structure switches, mRNA splicing, RNA export, translation, and miRNA biogenesis.[14,20,21] Moreover, RNA methylation also has been found in viral RNA, which impacts viral gene expression and has great potential for stimulating therapeutic developments.[22−25]

Received: September 13, 2020
Accepted: December 8, 2020
Published: December 17, 2020

https://dx.doi.org/10.1021/acschembio.0c00735
ACS Chem. Biol. 2021, 16, 76–85

Scheme 1. Synthesis of N^3-Methyl-Cytidine Phosphoramidite 10[a]

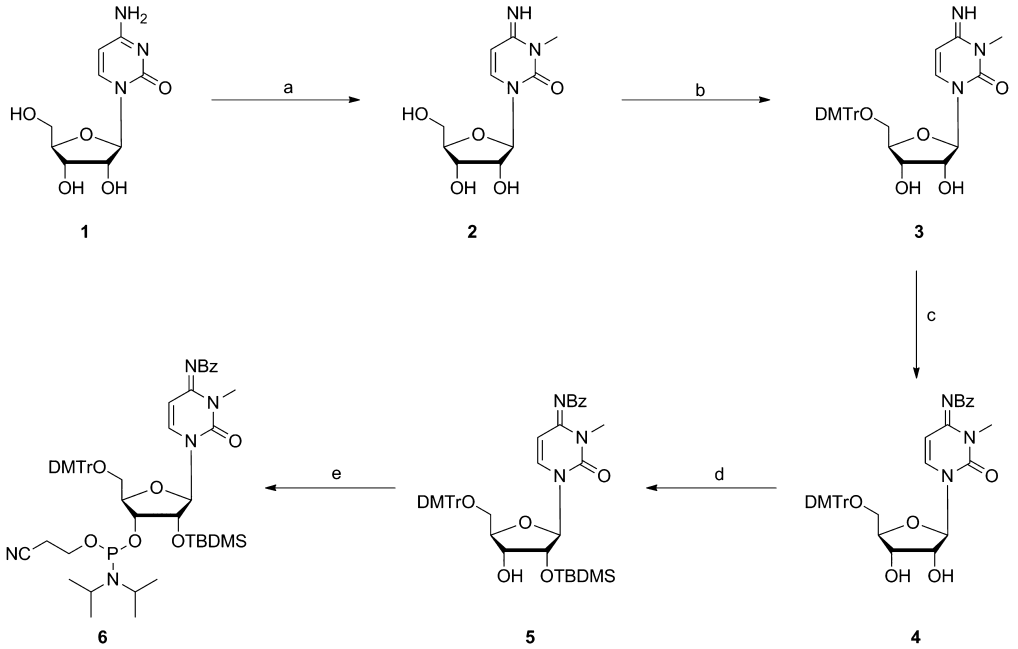

[a]Reagents and conditions: (a) MeI, DMF; (b) DMTrCl, Py; (c) TMSCl, Py; BzCl; (d) TBDMSCl, imidazole, DMF; (e) (i-$Pr_2N)_2P(Cl)OCH_2CH_2CN$, $(i\text{-Pr})_2$NEt, 1-methylimidazole, DCM.

N^3-Methylcytidine (m^3C) was first discovered in *Saccharomyces cerevisiae* total RNA[26] and later found in eukaryotic tRNA,[16,27−32] occuring most frequently in position 32 of the anticodon stem loops to impact tRNA structure, ribosome binding affinity and decoding activity. The working enzymes responsible for m^3C in tRNA are the methyltransferase Trm140 or the complex of Trm140 and Trm141 (METTL2 and METTL6). Recently, Fu and co-workers reported the new discovery of METTL8 as an mRNA m^3C writer enzyme and provided the first evidence of the existence of m^3C modification in the mRNA of mice and humans.[33,34] The m^3C modification may play versatile roles in impacting mRNA processing and biological functions. More interestingly, m^3C has been uniquely detected in the viral RNAs from Huh7, ZIKV, and DENV virions and the cells with these virus infections.[35] The m^3C modification also has the potential to be demethylated by eraser enzymes. Alkylation repair homologue 3 (ALKBH3), as well as its bacterial ancestor Alkb, have been shown to demethylate the m^3C in tRNA to affect RNA stability and prevent degradation.[36,37] ALKBH3 expression has also been linked to tumor progression and the regulation of protein synthesis, suggesting m^3C plays a prominent role in cancer biology.[38]

Although much effort went into the discovery and detection of m^3C, little is known about its fundamental properties and biological functions. Since the N^3-position directly participates in the Watson−Crick pairing, this methylation is expected to disrupt the C:G pair and reduce the base pairing fidelity of cytosine. In addition, the methyl group on m^3C might also regulate binding by RNA readers. Therefore, we hypothesize that the methylation at the N^3 position of cytidine is a cellular mechanism to modulate base pairing specificity and affect the efficiency and fidelity of transcription and reverse transcription, thus increasing RNA/DNA synthesis error rates, which could be beneficial to certain biological systems like viruses and cancer cells. To the best of our knowledge, no chemical synthesis and base-pairing studies of RNA oligonucleotides containing m^3C modification have been reported. In this work, we report the new chemical synthesis of m^3C phosphoramidite building block and its incorporation into RNA oligonucleotides. The subsequent base-pairing stability and specificity studies of RNA duplexes containing one and two m^3C residues at different positions support the idea that the m^3C decreases both duplex stability and base pairing discrimination between C:G pair and other mismatched pairs. Our molecular dynamic simulation study further provides detailed structural insights into the m^3C:G base pairing pattern in an RNA duplex. Furthermore, we used m^3C in reverse transcription assays *in vitro* in the presence of AMV-RT, HIV-1-RT, MMLV-RT, and MutiScribe-RT and found that this methylation could specify the C:A pair for some RT enzymes with low fidelity, which would induce the G to A changes. For reverse transcriptase enzymes with higher fidelity (i.e., AMV-RT), m^3C could completely shut down DNA synthesis.

RESULTS AND DISCUSSION

Chemical Synthesis of m^3C Phosphoramidite Building Block and Its Containing RNA Oligonucleotides. Although the synthesis of m^3C nucleosides has been achieved,[39,40] more general phosphoramidite building blocks are required to make different scales of RNA strands through the solid phase synthesis of oligonucleotides. We started the synthesis of m^3C from the commercially available cytidine (**1**, Scheme 1), which was directly methylated by using MeI without any base to obtain the m^3C nucleoside. The sequential protections of the 5′-hydroxyl group with the dimethoxyltrityl (DMTr) group and N^4 position with the benzoyl (Bz) group yielded compound **4**. Subsequently, the 2′-hydroxyl group was protected with a *tert*-butyldimethylsilyl (TBDMS) group to obtain compound **5**, which is the key intermediate to make the final phosphoramidite building block **6** for the oligonucleotides solid phase synthesis.

https://dx.doi.org/10.1021/acschembio.0c00735
ACS Chem. Biol. 2021, 16, 76−85

As expected, the m^3C phosphoramidite building block is well compatible with the solid phase synthesis conditions including the trichloroacetic acid (TCA) and oxidative iodine treatments, resulting in very similar coupling yields as the commercially available native phosphoramidites. They are also stable in the basic cleavage from the solid phase beads and the $Et_3N{\cdot}3HF$ treatment to remove TBDMS protecting groups during the RNA oligonucleotide deprotection and purification. As a demonstration, six RNA strands containing this modification have been synthesized and confirmed by ESI- or MALDI-MS, as shown in Table 1.

Table 1. RNA Sequences Containing m^3C

entry	RNA sequences	measured (calcd) m/z
ON1	5′-AAUGCm^{3}CGCACUG-3′	$[M + H]^+$ = 3807.5 (3807.6)
ON2	5′-GGACUm^{3}CCUGCAG-3′	$[M + H]^+$ = 3823.6 (3823.6)
ON3	5′-Um^{3}CGUACGA-3′	$[M + H]^+$ = 2523.1 (2522.4)
ON4	5′-GUAm^{3}CGUAC-3′	$[M + H]^+$ = 2522.5 (2522.4)
ON5	5′-CCGGm^{3}CGCCGG-3′	$[M + H]^+$ = 3203.7 (3203.5)
ON6	5′-CGCGAAUUm^{3}CGCG-3′	$[M + H]^+$ = 3823.6 (3823.6)

Thermal Denaturation and Base Pairing Studies of m^3C RNA Duplexes. We synthesized two sets of RNA strands to investigate the thermodynamic properties and base pairing specificity of m^3C containing RNA duplexes. The normalized T_m curves of native and modified RNA duplexes, [5′-GGACUXCUGCAG-3′ and 3′-CCUGAYGACGUC-5′] with Watson–Crick and other noncanonical base pairs (X pairs with Y), are shown in Figure 1. The detailed melting temperature data are summarized in Table 2. Compared to the native counterparts, m^3C-modified RNA duplexes showed dramatically decreased thermal stability. In the native C:G paired 12-mer duplexes (compare entry 2 and 7), the m^3C decreases the T_m by 19.7 °C, corresponding to a $\Delta G°$ reduction of 9.6 kcal/mol. Similarly, the noncanonical base paired (ex. C:A, C:U, and C:C) duplexes containing this modification also showed significantly lower melting temperatures. The T_m drops by 9.9 °C in the C:A mismatched duplex (entry 3 vs 8), 7.0 °C in the C:U mismatched one (entry 4 vs 9), and 4.0 °C for the C:C mismatched one (entry 5 vs 10), corresponding to the $\Delta G°$ reduction of 4.5, 4.2, and 2.5 kcal/mol, respectively.

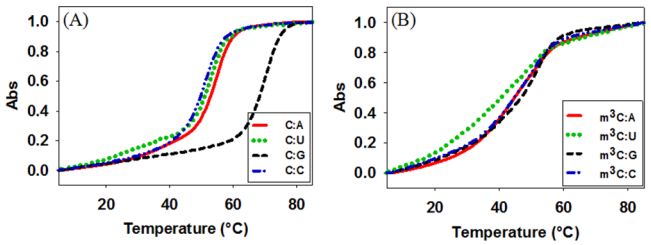

Figure 1. Normalized UV-melting curves of RNA duplexes. (A) Native sequence (5′-GGACUCCUGCAG-3′) pairs with matched and mismatched strands. (B) m^3C modification sequence (5′-GGACUm^{3}CCUGCAG-3′) pairs with matched and mismatched sequences.

These results indicate that m^3C modification significantly disrupts the C:G pair and the overall duplex stability. Indeed, when we compared this modification with the native C in a self-complementary 10-mer duplex context $(CCGGC^*GCCGG)_2$, where two consecutive m^3C:G's are introduced in the middle of the duplex, the T_m drops by 35.7 °C (entry 11 vs 12, Table 2), as shown in Figure S34. On the other hand, the comparison of base pairing specificity in this duplex system indicated that m^3C decreases the discrimination between the C:G pair and other mismatched C:A, C:U, and C:C pairs (entries 7–9, Table 2). The lowest T_m difference is 3.2 °C between the m^3C:G-duplex and the m^3C:C-one, and the highest T_m difference is only 5.6 °C between the m^3C:G-duplex and the m^3C:A-one. In comparison, in the nonmodified native RNA duplexes, these T_m differences vary from 15.4 to 18.9 °C (entries 2–5), dramatically bigger than the modified m^3C counterparts.

In addition, we also evaluated the impact of multiple m^3C modifications at different positions using a longer 22-mer RNA duplex template. As shown in Table 3 and Figure S35, the T_m of the RNA duplex containing a single m^3C residue at the C17 position (close to the 3′ end) drops by 5.5 °C (entry 2 vs 4, Table 3). In comparison, the T_m of the one containing two m^3C residues at C17 and C19 positions decreases by only 6.5 °C (entry 2 vs 4 vs 6, Table 3), meaning that the additional m^3C residue in the adjacent position has a small impact on duplex stability with only a 1.0 °C T_m decrease, and the further structural perturbation is "buffered" by the first m^3C modification. By contrast, separating the two m^3C modifications at C5 and C17 positions resulted in a dramatic drop of T_m by 37.2 °C (entry 2 vs 8, Table 3). While it has been

Table 2. Melting Temperatures of Native and m^3C-Modified RNA Duplexes

	entry	sequences	base pair	T_m (°C)[a]	ΔT_m (°C)[b]	$-\Delta G°$ (kcal/mol)[c]
Duplex-1	1	**I**: 5′-GGACU**C**CUGCAG-3′				
	2	**I** + 3′-CCUGA**G**GACAUC-5′	C:G	69.6		20.6
	3	**I** + 3′-CCUGA**A**GACAUC-5′	C:A	54.2	−15.4	14.0
	4	**I** + 3′-CCUGA**U**GACAUC-5′	C:U	52.9	−16.7	14.3
	5	**I**+ 3′-CCUGA**C**GACAUC-5′	C:C	50.7	−18.9	12.4
	6	**II**: 5′-GGACU**m^{3}C**CUGCAG-3′				
	7	**II** + 3′-CCUGA**G**GACAUC-5′	m^{3}C:G	49.9		11.0
	8	**II** + 3′-CCUGA**A**GACAUC-5′	m^{3}C:A	44.3	−5.6	9.5
	9	**II** + 3′-CCUGA**U**GACAUC-5′	m^{3}C:U	45.9	−4.0	10.1
	10	**II** + 3′-CCUGA**C**GACAUC-5′	m^{3}C:C	46.7	−3.2	9.9
Duplex-2	11	**III**: $(5'\text{-CCGG}\mathbf{C}\text{GCCGG-}3')_2$	C:G	74.6		18.3
	12	**IV**: $(5'\text{-CCGG}\mathbf{m^3C}\text{GCCGG-}3')_2$	m^{3}C:G	38.9	−35.7	7.8

[a]The T_m's were measured in sodium phosphate (10 mM, pH 7.0) buffer containing 100 mM NaCl, T_m values reported are the average of four measurements. [b]ΔT_m values are relative to the duplexes with only Watson–Crick pairs. [c]Obtained by nonlinear curve fitting using Meltwin 3.5.[41]

https://dx.doi.org/10.1021/acschembio.0c00735
ACS Chem. Biol. 2021, 16, 76–85

Table 3. Melting Temperatures of Native and m^{3}C-Modified 22-mer RNA Duplexes

entry	sequences	T_m (°C)[a]	ΔT_m (°C)[b]
1	**VII**: 5′-UGAGCUAGUAGGUUGUCUCGUU-3′		
2	**VII** + 3′-ACUCGAUCAUCCAACAGAGCAA-5′	71.7	
3	**VIII**: 5′-UGAGCUAGUAGGUUGUm^{3}CUCGUU-3′		
4	**VIII** + 3′-ACUCGAUCAUCCAACAGAGCAA-5′	66.2	−5.5
5	**IX**: 5′-UGAGCUAGUAGGUUGUm^{3}CUm^{3}CGUU-3′		
6	**IX** + 3′-ACUCGAUCAUCCAACAGAGCAA-5′	65.2	−6.5
7	**X**: 5′-UGAGm^{3}CUAGUAGGUUGUm^{3}CUCGUU-3′		
8	**X** + 3′-ACUCGAUCAUCCAACAGAGCAA-5′	34.5	−37.2

[a]The T_m's were measured in sodium phosphate (10 mM, pH 7.0) buffer containing 100 mM NaCl; T_m values reported are the average of four measurements. [b]ΔT_m values are relative to the native duplexes with only Watson−Crick pairs.

known that the RNA duplex structure is flexible to accommodate many different chemical modifications, the wide duplex stability range that m^{3}C could induce and the capability of fine-tuning T_m in a position-dependent manner might be useful for therapeutic applications, to enhance the efficacy of antisense and RNAi based mechanisms.

Molecular Simulation Studies of m^{3}C-RNA Duplex. In order to investigate more detailed structural insights into the base pairing patterns of the m^{3}C containing RNA duplex, we conducted molecular dynamic simulation studies. The results from the MD simulations are summarized in Figure 2. The RNA duplex was simulated in both canonical (C-G) and modified (m^{3}C-G) forms. We calculated the hydrogen-bonding distances between the donor−acceptor pairs for the canonical and modified base pairs from the ensemble of structures generated in the production run. The curves are moved vertically for visual clarity. The canonical C:G base pair retains all three hydrogen bonds throughout the simulation. However, in the modified m^{3}C-G pair, the m^{3}C rotates for about 45° to expose the methyl group into the major groove and avoid the clashing with N^1 of the pairing G. This conformational change, which might have an entropic penalty, allows for the single H-bond acceptor (O^2) to form bifurcated hydrogen bonds with N^1 and N^2 of guanine. The bifurcated hydrogen bonds also appear weaker as evidenced by higher average distances and fluctuations. Similar bonding patterns might also exist in other mis-matched pairs to minimize the discrimination of C to other bases. Since a bifurcated hydrogen bond is ∼50% as strong as the one−one hydrogen bond,[42] we estimate a loss of about two hydrogen bonds along with possible entropic losses, which is consistent with the significant weakening of duplex stability observed in our thermostability studies. When there are more m^{3}C residues present in the duplex, this kind of conformational flexibility caused by the base rotation and single hydrogen bonding might be able to accumulate and increase the stability "buffering effect" depending on the relative positions of m^{3}C residues, as the T_m data shown in Table 3.

Impacts of m^{3}C Modification on Reverse Transcription. In order to study the potential biological consequences of m^{3}C induced changes in hydrogen bonding during nucleic acid synthesis, we conducted reverse transcription assays *in vitro* using a modified-template directed primer extension reaction, as shown in Figure 3. The 5′-end of the DNA primer was labeled with the fluorescent FAM group, and a 31-nt-long modified RNA was used as the template, with the m^{3}C residue as the starting site of the extension reaction, which allows the direct view of the impacts of this modification to the whole reverse transcription complex. The reverse transcription yields or fidelity with different base pairing substrates in the presence of different reverse transcriptases were quantitated by the fluorescence gel images with single-nucleotide resolution (Figures 4−6) and the according UV images (Figures S36−S38).

The Avian Myeloblastosis Virus Reverse Transcriptase (AMV-RT) is a widely used RNA-directed DNA polymerase in RT-PCR and RNA sequencing with high fidelity.[43] When AMV-RT was used in the presence of different dNTP substrates with the native RNA template (Figure 4A), the reverse transcription reaction completed with all of the natural dNTPs (lane Nat). AMV-RT could only use dGTP for incorporation against the starting C residue on the template, while no other dNTPs could be added to the primer (lane A, T, G, C). For AMV-RT and an m^{3}C modified RNA template

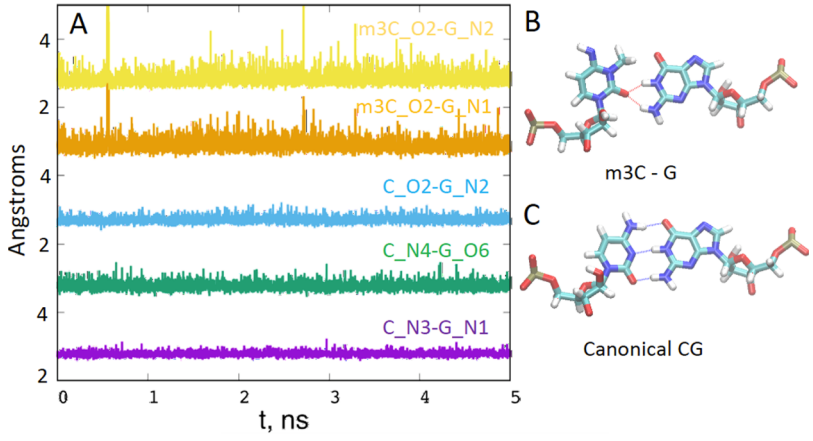

Figure 2. Molecular simulation results. The hydrogen bonding distances (A) vary at different time points in the RNA duplex containing m^{3}C:G (B) and native C:G (C) pairs.

https://dx.doi.org/10.1021/acschembio.0c00735
ACS Chem. Biol. 2021, 16, 76−85

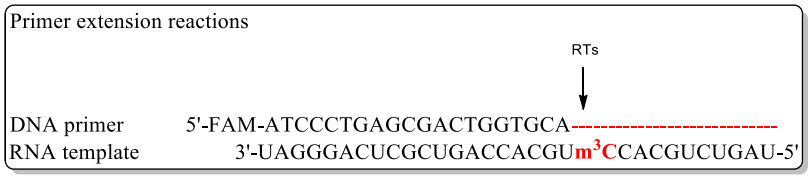

Figure 3. Primer extension reaction using m^3C modified RNA template.

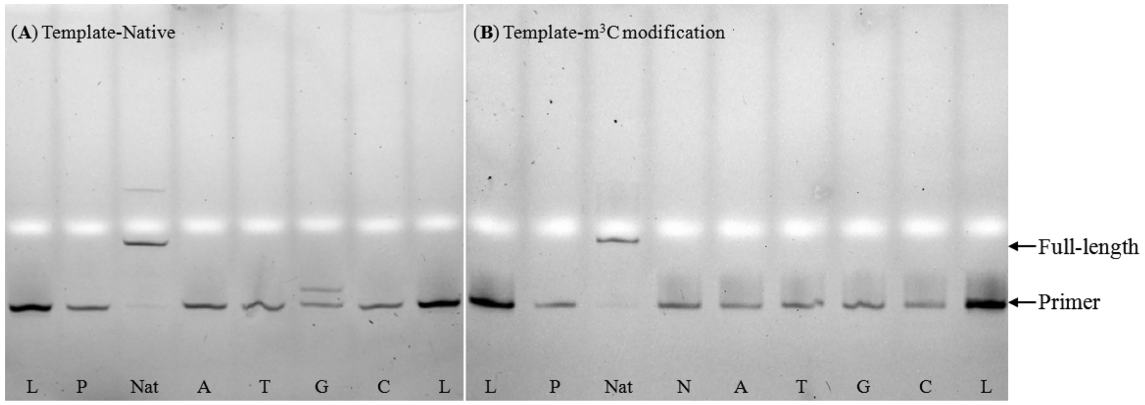

Figure 4. Fluorescent (A and B) gel images of standing-start primer extension reactions for AMV RT using an m^3C containing RNA template and the corresponding natural template. Lanes: L, ladder; P, primer; Nat, natural template with all four dNTPs; A, T, G, and C, reactions in the presence of the respective dNTP; N, reactions in the presence of all four dNTPs.

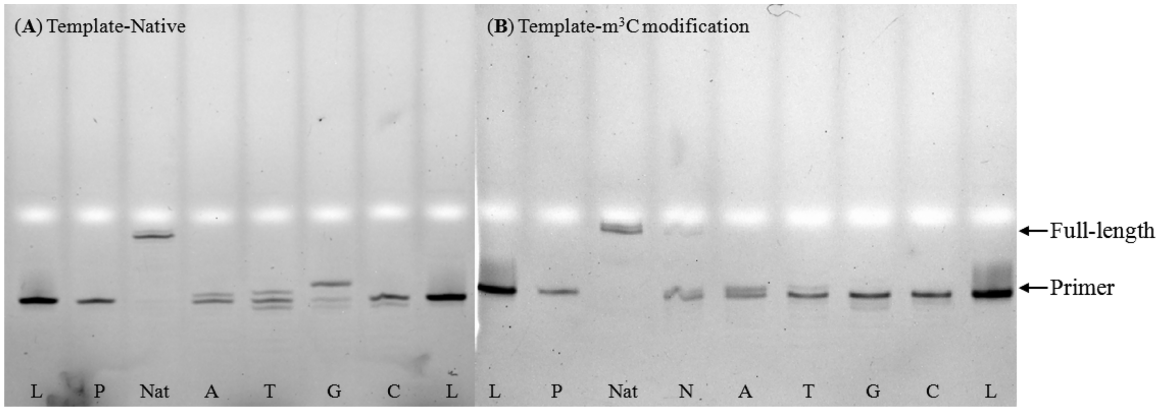

Figure 5. Fluorescent (A and B) gel images of standing-start primer extension reactions for HIV-1 RT using m^3C containing RNA template and the corresponding natural template. Lanes: L, ladder; P, primer; Nat, natural template with all four dNTPs; A, T, G, and C, reactions in the presence of the respective dNTP; N, reactions in the presence of all four dNTPs.

(Figure 4B), no full-length product was observed even in the presence of all the natural dNTPs (lane Nat vs N), indicating that this single m^3C modification template completely inhibits the AMV-RT activity. Our observation is also consistent with the report that m^3C acts as an RT stop residue in RT-based techniques.[44]

By contrast, when the HIV-1-RT, which has relatively lower replication fidelity than AMV-RT, was used, it dramatically increased incorporation yield when dGTP was used as the dNTP (Figure 5A, lane G). We also observed that misincorporation of dATP and dTTP, but not dCTP, was present when using the HIV-1-RT (lane A, T, and C). In the presence of the m^3C modified template (Figure 5B), we observed a very small trace amount of full-length product (less than 5%) in the presence of all natural dNTPs (lanes Nat and N), supporting the idea that a single m^3C modification severely inhibits the HIV-1-RT activity and results in a very low reaction yield. Interestingly, the m^3C modification totally inhibits dGTP and dTTP incorporation but significantly increases the dATP incorporation yield (lanes A, T, and G), resulting in the order of preferential incorporation efficiency as A ≫ T > G, C.

Subsequently, we explored the impacts of m^3C on MMLV-RT, another enzyme with replication fidelity lower than AMV but higher than HIV-1 RT.[45] MMLV-RT together with the native RNA template (Figure 6A) in the reverse transcription reaction gives normal full length product in the presence of all the natural dNTPs (lane Nat). Although very high dGTP incorporation efficiency (lane G) was observed for MMLV-RT, the misincorporation of dATP was extremely high (lane A), supporting the idea that MMLV-RT can recognize and well accommodate the C:A pair in the reverse transcription complex. Similarly, dTTP was also incorporated into the primer strand with a medium yield (lane T). On the other hand, the presence of m^3C in the template inhibits the normal enzyme activity of MMLV-RT (Lane N and G in Figure 6B), resulting in a mixture of three major strands in the reaction

https://dx.doi.org/10.1021/acschembio.0c00735
ACS Chem. Biol. 2021, 16, 76−85

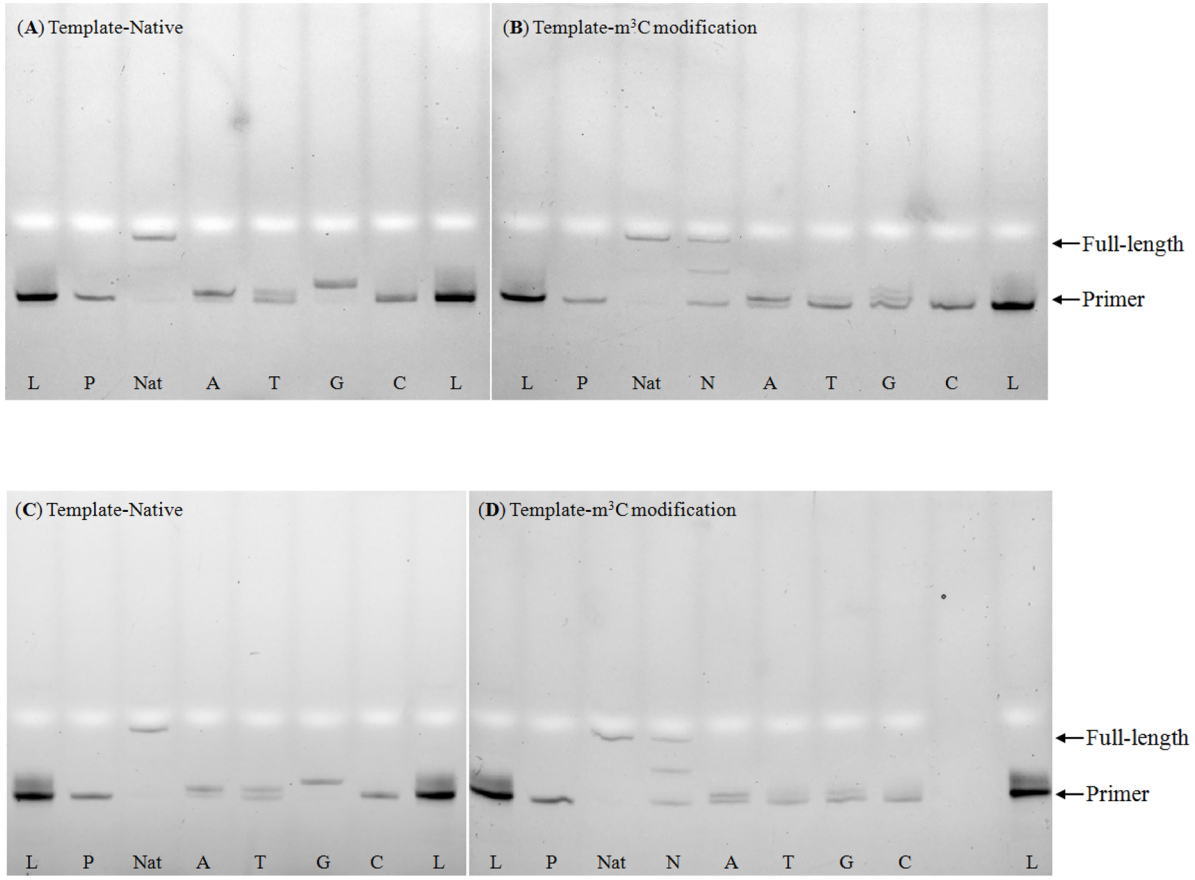

Figure 6. Fluorescent gel images of standing-start primer extension reactions for MMLV RT (A and B) and MultiScribe RT (C and D) using m^3C containing RNA templates and the corresponding natural templates. Lanes: L, ladders; P, primer; Nat, natural template with all four dNTPs; A, T, G, and C, reactions in the presence of the respective dNTP; N, reactions in the presence of all four dNTPs.

system, although the full-length product inhibition is much lower than the HIV-1 RT system. However, the m^3C template modification does not impact the incorporation of dATP. As a result, a similar dNTP's incorporation efficiency order, A ≫ T, G > C, as HIV-1 RT, was observed for MMLV-RT. Furthermore, when the MutiScribe RT, a recombinant version of MMLV RT, was applied to the system, very similar results were obtained (Figure 6C and D).

Many base modifications that do not change the Watson−Crick base pairing pattern have big impacts on the activity and fidelity of RNA polymerases, with m^6A, m^5C, m^5U, and hm^5U being examples.[46] The accuracy or fidelity of the base incorporation against a specific modified base on the template strand used for reverse transcription as well as the overall DNA or RNA synthesis error rates remains largely unestablished for many RNA modifications. HIV-1 RT is known as a low fidelity reverse transcriptase that catalyzes nucleotide mismatches with an error frequency of 1/2000 to 1/4000 and prefers a C:A pair over other mismatches, which frequently results in a G-to-A mutation during HIV gene replication.[47] Our results suggest that although the HIV-1 RT can induce both C:A and C:T pairs using an unmodified template, the presence of the m^3C modification largely enhances the C:A pair while inhibiting the C:T one. We also observed that MMLV RT and MutiScribe RT enhance the C:A pair while inhibiting the C:T one. Our results support the idea that the m^3C modification could specify the C:A pair in the presence of lower fidelity reverse transcriptases, thus further increasing the G-to-A changes during reverse transcription. In contrast, the m^3C encountered by enzymes with higher fidelity (i.e., AMV-RT) does not specify A or induce any other base mismatch, and primary serves as an RT stop.

We do note that the overall replication using HIV-1 RT is significantly (>90%) inhibited in the presence of m^3C on the template, very similar to the AMV-RT case, which completely inhibits the DNA synthesis. One would expect a lower-fidelity RNA polymerase like HIV-1 to better accommodate the unnatural base pairs and promote higher replication yields when compared to the higher-fidelity AMV-RT. Indeed, both MMLV RT and MutiScribe RT, which have a fidelity between HIV-1 RT and AMV-RT, show partial inhibition and result in a 50% of full-length product. Although there is no evidence that m^3C modification exists in te HIV-1 virus, our study provides the potential support that the m^3C modification may have unique effects on HIV-1 RT and allows the virus to regulate gene replication during different environmental selection stresses, which could be exploited to develop molecular tools for mapping the m^3C in different RNA contexts and new therapeutics for HIV. Furthermore, the downstream demethylation process of m^3C catalyzed by ALKBH3 may also play roles in restoring base pairing fidelity during virus replication, therefore representing another potential target in developing RNA based antiviral drugs.

https://dx.doi.org/10.1021/acschembio.0c00735
ACS Chem. Biol. 2021, 16, 76−85

CONCLUSION

In summary, we synthesized the m^{3}C phosphoramidite and a series of RNA oligonucleotides containing the modification. Our base-pairing and specificity studies show that the m^{3}C modification disrupts the C:G pair and significantly decreases RNA duplex stability, which also results in the loss of base pairing discrimination of the C:G pair with C:A, C:T, and C:C mismatched pairs. We also demonstrated that introducing two m^{3}C modifications in the same sides (5′ or 3′ side) provided a relatively smaller effect on T_m compared to one modification. On the contrary, separating the two modifications could significantly reduce the duplex stability. Our molecular dynamic simulation study further reveals the detailed structural insights into the m^{3}C:G base pairing pattern in the RNA duplex. In addition, our investigation of this methylation effect on the reverse transcription model *in vitro* demonstrated that the m^{3}C modification could specify the C:A pair for some RT enzymes, which would induce the G to A changes if used by low fidelity enzymes. For reverse transcriptase enzymes with higher fidelity (i.e., AMV-RT), m^{3}C could completely shut down DNA synthesis. Our work provides detailed insights into the thermostability and the biological importance of m^{3}C in RNA. Further, it provides a foundation for developing new molecular tools for mapping m^{3}C in different RNA contexts and exploring the biochemical and biomedical potentials of m^{3}C in the design and development of RNA based therapeutics.

EXPERIMENTAL SECTION

Materials and General Procedures of Synthesis. Anhydrous solvents were used and redistilled using standard procedures. All solid reagents were dried under a high vacuum line prior to use. Air sensitive reactions were carried out under argon. RNase-free water, tips, and tubes were used for RNA purification and thermodynamic studies. Analytical TLC plates precoated with silica gel F254 (Dynamic Adsorbents) were used for monitoring reactions and visualized by UV light. Flash column chromatography was performed using silica gel (32−63 μm). All ^{1}H, ^{13}C, and ^{31}P NMR spectra were recorded on a Bruker 400 and 500 MHz spectrometer. Chemical shift values are in parts per million. ^{13}C NMR signals were determined by using the APT technique. High-resolution MS were achieved by ESI at the University at Albany, SUNY.

Synthesis of m^{3}C Phosphoramidites. *3-N-Methyl-cytidine* ***2***. To a solution of cytidine **1** (4.86 g, 20 mmol) in dry DMF (50 mL) was added iodomethane (2.5 mL, 40 mmol), and the solution was kept at RT for 24 h. DMF was evaporated; the residue was evaporated with toluene (2 × 100 mL) and dissolved in acetone (20 mL). Hexane (50 mL) was added to the solution, and the resulting mixture was kept at −20 °C for 1 h. The precipitate was filtered, washed with a cold mixture of acetone/hexane (v/v = 1:1; 2 × 50 mL). The solid was dried in a vacuum to give compound **2** (3.6 g, 14 mmol, 70% yield) as a yellow solid. ^{1}H NMR (500 MHz, DMSO-d_6): δ 9.79 (br, 1H), 9.15 (br, 1H), 8.31 (d, J = 7.5 Hz, 1H), 6.20 (d, J = 8.0 Hz, 1H), 5.70 (d, J = 3.5 Hz, 1H), 5.51 (br, 1H), 5.17 (br, 1H), 4.05−4.03 (m, 1H), 3.95−3.89 (m, 2H), 3.73 (dd, J = 2.5, 12.5 Hz, 1H), 3.60 (dd, J = 2.5, 12.0 Hz, 1H), 3.35 (s, 3H). ^{13}C NMR (125 MHz, $CDCl_3$): δ 159.4, 148.1, 142.1, 94.5, 91.2, 85.1, 74.6, 69.0, 60.2, 31.2. HRMS (ESI-TOF) $[M + H]^+$ = 258.1090 (calc. 258.1090). Chemical formula: $C_{10}H_{15}N_3O_5$.

1-(5′-O-4,4′-Dimethoxytrityl-beta-D-ribofuranosyl)-3-N-methyl-cytidine, ***3***. To a solution of compound **2** (3.5 g, 13.6 mmol) in dry pyridine (40 mL) was added 4,4′-dimethoxytrityl chloride (6.9 g, 20.4 mmol). The resulting solution was stirred at RT overnight. To the suspension was added CH_2Cl_2 (200 mL), and the organic layer was subsequently washed with 5% aqueous $Na_2S_2O_3$ (2 × 100 mL), sat. aqueous sodium bicarbonate (100 mL), and brine (100 mL). The organic layer was dried by anhydrous sodium sulfate, filtered, and evaporated under reduced pressure. The residue was purified by silica gel chromatography to give compound **3** (3.9 g, 5.9 mmol, 43% yield) as a white solid. TLC R_f = 0.2 (10% MeOH in CH_2Cl_2). ^{1}H NMR (400 MHz, $CDCl_3$): δ 7.61 (d, J = 8.0 Hz, 1H), 7.39−7.36 (m, 2H), 7.28−7.16 (m, 7H), 6.82−6.79 (m, 4H), 5.86 (d, J = 3.2 Hz, 1H), 5.76 (d, J = 7.2 Hz, 1H), 4.36−4.30 (m, 2H), 4.18 (m, 1H), 3.73 (d, 6H), 3.48−3.40 (m, 5H). ^{13}C NMR (125 MHz, $CDCl_3$): δ 158.9, 158.6, 149.4, 149.37, 144.5, 135.5, 135.3, 130.2, 128.2, 128.0, 113.3, 98.2, 90.9, 86.9, 83.5, 74.9, 69.9, 62.5, 55.3, 30.3. HRMS (ESI-TOF) $[M + H]^+$ = 560.2390 (calc. 560.2397). Chemical formula: $C_{31}H_{33}N_3O_7$.

1-(5′-O-4,4′-Dimethoxytrityl-beta-D-ribofuranosyl)-4-N-benzoyl-3-N-methyl-cytidine, ***4***. Compound **3** (2.3 g, 4.2 mmol) was coevaporated with pyridine (2 × 50 mL) and redissolved in pyridine (50 mL). Trimethylsilyl chloride (TMSCl) (2.1 mL, 16.8 mmol) was added, and the mixture was stirred at RT for 1 h whereupon benzoyl chloride (BzCl; 0.84 mL, 5.04 mmol) was added. The resulting solution was stirred for 4 h at RT whereupon water (10 mL) was added. After stirring for 5 min at RT, aqueous ammonia (15 mL, 15.8 M) was added, and the mixture was stirred for 15 min at RT and then evaporated to dryness under reduced pressure. The residue was purified by silica gel chromatography to give compound **4** (2.3 g, 3.47 mmol, 82% yield) as a white solid. TLC R_f = 0.4 (50% EtOAc in CH_2Cl_2). ^{1}H NMR (400 MHz, $CDCl_3$): δ 8.15−8.12 (m, 2H), 7.64 (d, J = 8.4 Hz, 1H),7.56−7.51 (m, 1H), 7.46−7.42 (m, 2H), 7.35−7.33 (m, 2H), 7.29−7.18 (m, 8H), 6.84−6.80 (m, 4H), 6.25 (d, J = 8.4 Hz, 1H), 5.82 (d, J = 3.6 Hz, 1H), 4.37−4.26 (m, 3H), 3.78 (d, 6H), 3.58 (s, 3H), 3.48 (dd, J = 2.8 Hz, 10.8 Hz, 1H), 3.38 (dd, J = 3.2 Hz, 10.8 Hz, 1H). ^{13}C NMR (125 MHz, $CDCl_3$): δ 177.4, 158.7, 151.1, 144.1, 135.8, 135.7, 135.4, 135.2, 132.5, 130.1, 130.0, 129.7, 128.2, 128.1, 128.0, 127.1, 113.31, 113.30, 98.2, 91.5, 87.1, 84.3, 76.2, 70.5, 62.2, 55.2, 30.0. HRMS (ESI-TOF) $[M + H]^+$ = 664.2646 (calc. 664.2659). Chemical formula: $C_{38}H_{37}N_3O_8$.

1-(2′-O-tert-Butyldimethylsilyl-5′-O-4,4′-dimethoxytrityl-beta-D-ribofuranosyl)-4-N-benzoyl-3-N-methyl-cytidine ***5***. Compound **4** (1.3 g, 2 mmol) was dissolved in dry DMF (12 mL), then *tert*-butyldimethylsilyl chloride (TBDMSCl, 362 mg, 2.4 mmol) and imidazole (272 mg, 4 mmol) were added into the solution. The resulting solution was stirred overnight at RT. The solution was diluted with EtOAc (200 mL) and washed with brine (2 × 100 mL). The organic layer was dried by anhydrous sodium sulfate, filtered, and evaporated under reduced pressure. The residue was purified by silica gel chromatography to give compound **5** (600 mg, 0.77 mmol, 39% yield) as a white solid. TLC R_f = 0.6 (hexane/EA = 1:1). ^{1}H NMR (500 MHz, $CDCl_3$): δ 8.15−8.12 (m, 2H), 7.82 (d, J = 8.5 Hz, 1H), 7.55−7.50 (m, 1H), 7.46−7.42 (m, 2H), 7.38−7.35 (m, 2H), 7.29−7.25 (m, 6H), 7.22−7.16 (m, 1H), 6.85−6.82 (m, 4H), 6.08 (d, J = 8.0 Hz, 1H), 5.94 (d, J = 2.5 Hz, 1H), 4.38−4.33 (m, 1H), 4.29−4.27 (m, 1H), 4.09−4.06 (m, 1H), 3.78 (d, J = 1.0 Hz, 6H), 3.55 (s, 3H), 3.57−3.46 (m, 2H), 0.94 (s, 9H), 0.24 (s, 3H), 0.18 (s, 3H). ^{13}C NMR (125 MHz, $CDCl_3$): δ 177.3, 158.7, 155.7, 150.3, 144.1, 136.0, 135.9, 135.4, 135.2, 132.4, 130.1, 130.0, 129.7, 128.20, 128.19, 128.0, 127.2, 98.1, 89.8, 87.1, 83.3, 76.8, 69.8, 61.9, 55.2, 30.0, 25.8, 18.1, −4.5, −5.2. HRMS (ESI-TOF) $[M + H]^+$ = 778.3527 (calc. 778.3524). Chemical formula: $C_{44}H_{51}N_3O_8Si$.

1-[2′-O-tert-Butyldimethylsilyl-3′-O-(2-cyanoethyl-N,N-diisopropylamino)phosphoramidite-5′-O-(4,4′-dimethoxytrityl-beta-D-ribofuranosyl)]-4-N-benzoyl-3-N-methyl-cytidine ***6***. To a solution of compound **5** (600 mg, 0.77 mmol) in dry DCM (13 mL) was added N,N-di-iso-propylethylamine (0.38 mL, 3.08 mmol) and 2-cyanoethyl *N,N*-diisopropylchlorophosphoramidite (0.23 mL, 1.54 mmol). The resulting solution was stirred overnight at RT under argon gas. The reaction was quenched with water and extracted with ethyl acetate. After drying the organic layer over Na_2SO_4 and evaporation, the residue was purified by silica gel chromatography to give compound **6** (500 mg, 0.51 mmol, 66% yield) as a white solid. TLC R_f = 0.6 (hexane/EA = 1:1). ^{1}H NMR (400 MHz, $CDCl_3$): δ 8.15−8.12 (m, 2H), 7.90−7.19 (m, 13H), 6.84−6.80 (m, 4H), 6.16−5.91 (m, 2H), 4.38−3.91 (m, 3H), 3.78 (s, 6H), 3.61−3.36 (m, 7H),

https://dx.doi.org/10.1021/acschembio.0c00735
ACS Chem. Biol. 2021, 16, 76−85

2.67−2.37 (m, 2H), 2.06−2.04 (m, 1H), 1.29−1.14 (m, 12H), 1.02−0.98 (m, 3H), 0.93−0.9 (m, 9H), 0.19−0.13 (m, 6H). ^{31}P NMR (162 MHz, $CDCl_3$): δ 149.97, 148.94. HRMS (ESI-TOF) $[M + H]^+$ = 978.4561 (calc. 978.4602). Chemical formula: $C_{53}H_{68}N_5O_9PSi$.

Synthesis and Purification of m^{3}C Containing RNA Oligonucleotides. All oligonucleotides were chemically synthesized on 1.0 μmol scales by solid phase synthesis using the Oligo-800 synthesizer. The m^{3}C phosphoramidite was dissolved in acetonitrile to a concentration of 0.1 M. I_2 (0.02 M) in THF/Py/H_2O solution was used as an oxidizing reagent. Coupling was carried out using 5-ethylthio-1H-tetrazole solution (0.25 M) in acetonitrile for 12 min, for both native and modified phosphoramidites. About 3% trichloroacetic acid in methylene chloride was used for the 5′-detritylation. Synthesis was performed on control-pore glass (CPG-500) immobilized with the appropriate nucleoside through a succinate linker. All the reagents used are standard solutions obtained from the ChemGenes Corporation. The oligonucleotide was prepared in DMTr off form. After synthesis, the oligos were cleaved from the solid support and fully deprotected with 1:1 v/v ammonium hydroxide solution (28% NH_3 in H_2O) and methylamine (40% w/w aqueous solution) at 65 °C for 45 min. The solution was evaporated to dryness using a Speed-Vac concentrator. The solid was dissolved in 100 μL of DMSO and was desilylated using a triethylamine trihydrogen fluoride ($Et_3N{\cdot}3HF$) solution at 65 °C for 2.5 h. Cooled down to RT, the RNA was precipitated by adding 0.025 mL of 3 M sodium acetate and 1 mL of ethanol. The solution was cooled to −80 °C for 1 h before the RNA was recovered by centrifugation and finally dried under a vacuum.

The oligonucleotides were purified by IE-HPLC at a flow rate of 1 mL/min. Buffer A was 20 mM Tris-HCl, pH 8.0; buffer B was 1.25 M NaCl in 20 mM Tris-HCl, pH 8.0. A linear gradient from 100% buffer A to 70% buffer B in 20 min was used to elute the oligos. The analysis was carried out by using the same type of analytical column with the same eluent gradient. All the modified oligos were checked by MALDI MS. The 22-mer and 31-mer RNA oligonucleotides were purified on a preparative 20% denaturing polyacrylamide gel (PAGE).

UV-Melting Temperature (T_m) Study. Solutions of the duplex RNAs (1.5 μM) were prepared by dissolving the purified RNAs in sodium phosphate (10 mM, pH 7.0) buffer containing 100 mM NaCl. The solutions were heated to 95 °C for 5 min, then cooled down slowly to RT and stored at 4 °C for 2 h before T_m measurement. Thermal denaturation was performed in a Cary 300 UV−visible spectrophotometer with a temperature controller. The temperature reported is the block temperature. Each denaturizing curve was acquired at 260 nm by heating and cooling from 5 to 80 °C four times at a rate of 0.5 °C/min. All the melting curves were repeated at least four times. The thermodynamic parameter of each strand was obtained by fitting the melting curves using the Meltwin software.

Molecular Dynamic Simulation Studies. To study the m^{3}C modification in the context of the RNA duplex in MD simulations, we developed AMBER[48] type force-field parameters for the atoms of the modified nucleoside. We used the AM1-BCC[49] charge model to calculate the atomic charges, which is developed as a fast yet accurate alternate for ESP-fit using Hartree−Fock theory and 6-31G* basis sets.[50] AMBER99 force-field parameters were used for bonded interactions,[48] and AMBER99 parameters with Chen-Garcia corrections[51] for the bases were used for LJ interactions. The unmodified RNA duplex was constructed in a-form using the Nucleic Acid Builder (NAB) suite of AMBER and mutated to create the modification.

Molecular dynamics simulations were performed using the Gromacs-2018 package.[52] The simulation system included the RNA duplex in water in a 3D periodic box. The initial box size was 4.0 × 4.0 × 6.0 nm^3 containing the RNA duplex, 3060 water molecules, and 22 neutralizing Na^+ ions. The system was subjected to energy minimization to prevent any overlap of atoms, followed by a 1 ns equilibration run. The equilibrated system was then subjected to a 100 ns production run. The MD simulations incorporated a leapfrog algorithm with a 2 fs time step to integrate the equations of motion. The system was maintained at 300 K and 1 bar, using the velocity rescaling thermostat[53] and Parrinello−Rahman barostat,[54] respectively. The long-ranged electrostatic interactions were calculated using the particle mesh Ewald (PME)[55] algorithm with a real space cutoff of 1.2 nm. LJ interactions were also truncated at 1.2 nm. The TIP3P model[56] was used represent the water molecules, and the LINCS[57] algorithm was used to constrain the motion of hydrogen atoms bonded to heavy atoms. Coordinates of the RNA molecule were stored every 20 ps for further analysis.

Reverse Transcription (RT) Assays. RT assays were performed with AMV RT (ThermoFisher), HIV-1 RT (AS ONE Corp.), MMLV RT (ThermoFisher), and MutiScribe RT (ThermoFisher) in 20 μL of total solution containing 10× reverse transcription buffer: 50 mM Tris (pH 8.3), 75 mM KCl, 3 mM $MgCl_2$, and 10 mM DTT. Final reaction mixtures contained an RNA template (5 μM), DNA FAM-primer (2.5 μM), and dNTP (1 mM). After the addition of an Rnase inhibitor (20 U) and each RT, AMV RT (10 U), HIV-1 RT (4 U), MMLV (100 U), and MutiScribe (50 U), the mixtures were incubated at 37 °C for 1 h. The reactions were quenched with stop solution [98% formamide, 0.05% xylene cyanol (FF), and 0.05% bromophenol blue], heated to 90 °C for 5 min, and then cooled to 0 °C in an ice bath. The reactions were analyzed by 15% PAGE 8 M urea at 250 V for 1−1.5 h. The fluorescent and UV gel imaging were done on a Bio-Rad Gel XR+ imager.

■ ASSOCIATED CONTENT

Supporting Information

The Supporting Information is available free of charge at https://pubs.acs.org/doi/10.1021/acschembio.0c00735.

Experimental procedures, spectral data, UV-melting curves, and PAGE gel UV images (PDF)

■ AUTHOR INFORMATION

Corresponding Author

Jia Sheng − *Department of Chemistry and The RNA Institute, University at Albany, State University of New York, Albany, New York 12222, United States*; orcid.org/0000-0001-6198-390X; Email: jsheng@albany.edu

Authors

Song Mao − *Department of Chemistry and The RNA Institute, University at Albany, State University of New York, Albany, New York 12222, United States*

Phensinee Haruehanroengra − *Department of Chemistry and The RNA Institute, University at Albany, State University of New York, Albany, New York 12222, United States*

Srivathsan V. Ranganathan − *The RNA Institute, University at Albany, State University of New York, Albany, New York 12222, United States*

Fusheng Shen − *Department of Chemistry and The RNA Institute, University at Albany, State University of New York, Albany, New York 12222, United States*

Thomas J. Begley − *The RNA Institute and Department of Biological Science, University at Albany, State University of New York, Albany, New York 12222, United States*

Complete contact information is available at: https://pubs.acs.org/10.1021/acschembio.0c00735

Notes

The authors declare no competing financial interest.

■ ACKNOWLEDGMENTS

We are grateful to NSF (CHE-1845486, MCB-1715234 and CHE-1726724) and the New Emerging Frontiers Research (NERF) grant from the University at Albany, State University

of New York for the financial support. We thank Z. Huang and C. Chen for their help in MS-Spec experiments.

REFERENCES

(1) Nachtergaele, S., and He, C. (2017) The emerging biology of RNA post-transcriptional modifications. *RNA Biol. 14*, 156−163.
(2) Boccaletto, P., Machnicka, M. A., Purta, E., Piatkowski, P., Baginski, B., Wirecki, T. K., de Crecy-Lagard, V., Ross, R., Limbach, P. A., Kotter, A., Helm, M., and Bujnicki, J. M. (2018) MODOMICS: a database of RNA modification pathways. 2017 update. *Nucleic Acids Res. 46*, D303−D307.
(3) Basanta-Sanchez, M., Temple, S., Ansari, S. A., D'Amico, A., and Agris, P. F. (2016) Attomole quantification and global profile of RNA modifications: Epitranscriptome of human neural stem cells. *Nucleic Acids Res. 44*, No. e26.
(4) Machnicka, M. A., Milanowska, K., Osman Oglou, O., Purta, E., Kurkowska, M., Olchowik, A., Januszewski, W., Kalinowski, S., Dunin-Horkawicz, S., Rother, K. M., Helm, M., Bujnicki, J. M., and Grosjean, H. (2012) MODOMICS: a database of RNA modification pathways−2013 update. *Nucleic Acids Res. 41*, D262−267.
(5) Cantara, W. A., Crain, P. F., Rozenski, J., McCloskey, J. A., Harris, K. A., Zhang, X., Vendeix, F. A., Fabris, D., and Agris, P. F. (2011) The RNA Modification Database, RNAMDB: 2011 update. *Nucleic Acids Res. 39*, D195−201.
(6) Wu, Y., Tang, Y., Dong, X., Zheng, Y. Y., Haruehanroengra, P., Mao, S., Lin, Q., and Sheng, J. (2020) RNA Phosphorothioate Modification in Prokaryotes and Eukaryotes. *ACS Chem. Biol. 15*, 1301−1305.
(7) Holley, R. W., Apgar, J., Everett, G. A., Madison, J. T., Marquisee, M., Merrill, S. H., Penswick, J. R., and Zamir, A. (1965) Structure of a Ribonucleic Acid. *Science 147*, 1462−1465.
(8) Holley, R. W., Everett, G. A., Madison, J. T., and Zamir, A. (1965) Nucleotide Sequences in the Yeast Alanine Transfer Ribonucleic Acid. *J. Biol. Chem. 240*, 2122−2128.
(9) Roundtree, I. A., Evans, M. E., Pan, T., and He, C. (2017) Dynamic RNA Modifications in Gene Expression Regulation. *Cell 169*, 1187−1200.
(10) Jiang, Q., Crews, L. A., Holm, F., and Jamieson, C. H. M. (2017) RNA editing-dependent epitranscriptome diversity in cancer stem cells. *Nat. Rev. Cancer 17*, 381−392.
(11) Hori, H. (2014) Methylated nucleosides in tRNA and tRNA methyltransferases. *Front. Genet. 5*, 144.
(12) Nachtergaele, S., and He, C. (2018) Chemical Modifications in the Life of an mRNA Transcript. *Annu. Rev. Genet. 52*, 349−372.
(13) Mongan, N. P., Emes, R. D., and Archer, N. (2019) Detection and analysis of RNA methylation. *F1000Research 8*, 559.
(14) Song, J., and Yi, C. (2017) Chemical Modifications to RNA: A New Layer of Gene Expression Regulation. *ACS Chem. Biol. 12*, 316−325.
(15) Sergiev, P. V., Aleksashin, N. A., Chugunova, A. A., Polikanov, Y. S., and Dontsova, O. A. (2018) Structural and evolutionary insights into ribosomal RNA methylation. *Nat. Chem. Biol. 14*, 226−235.
(16) Clark, W. C., Evans, M. E., Dominissini, D., Zheng, G., and Pan, T. (2016) tRNA base methylation identification and quantification via high-throughput sequencing. *RNA 22*, 1771−1784.
(17) Shi, H., Wei, J., and He, C. (2019) Where, When, and How: Context-Dependent Functions of RNA Methylation Writers, Readers, and Erasers. *Mol. Cell 74*, 640−650.
(18) Fu, Y., Dominissini, D., Rechavi, G., and He, C. (2014) Gene expression regulation mediated through reversible m(6)A RNA methylation. *Nat. Rev. Genet. 15*, 293−306.
(19) Wang, X., Lu, Z., Gomez, A., Hon, G. C., Yue, Y., Han, D., Fu, Y., Parisien, M., Dai, Q., Jia, G., Ren, B., Pan, T., and He, C. (2014) N6-methyladenosine-dependent regulation of messenger RNA stability. *Nature 505*, 117−120.
(20) Desrosiers, R., Friderici, K., and Rottman, F. (1974) Identification of methylated nucleosides in messenger RNA from Novikoff hepatoma cells. *Proc. Natl. Acad. Sci. U. S. A. 71*, 3971−3975.
(21) Zaccara, S., Ries, R. J., and Jaffrey, S. R. (2019) Reading, writing and erasing mRNA methylation. *Nat. Rev. Mol. Cell Biol. 20*, 608−624.
(22) Wu, L. (2019) HIV Evades Immune Surveillance by Methylation of Viral RNA. *Biochemistry 58*, 1699−1700.
(23) Chen, B., Li, Y., Song, R. F., Xue, C., and Xu, F. (2019) Functions of RNA N6-methyladenosine modification in cancer progression. *Mol. Biol. Rep. 46*, 1383−1391.
(24) Lichinchi, G., Zhao, B. S., Wu, Y., Lu, Z., Qin, Y., He, C., and Rana, T. M. (2016) Dynamics of Human and Viral RNA Methylation during Zika Virus Infection. *Cell Host Microbe 20*, 666−673.
(25) Ciuffi, A. (2016) Viral cell biology: HIV RNA gets methylated. *Nat. Microbiol. 1*, 16037.
(26) Hall, R. H. (1963) Isolation of 3-Methyluridine and 3-Methylcytidine from Solubleribonucleic Acid. *Biochem. Biophys. Res. Commun. 12*, 361−364.
(27) Cozen, A. E., Quartley, E., Holmes, A. D., Hrabeta-Robinson, E., Phizicky, E. M., and Lowe, T. M. (2015) ARM-seq: AlkB-facilitated RNA methylation sequencing reveals a complex landscape of modified tRNA fragments. *Nat. Methods 12*, 879−884.
(28) D'Silva, S., Haider, S. J., and Phizicky, E. M. (2011) A domain of the actin binding protein Abp140 is the yeast methyltransferase responsible for 3-methylcytidine modification in the tRNA anti-codon loop. *RNA 17*, 1100−1110.
(29) Han, L., Marcus, E., D'Silva, S., and Phizicky, E. M. (2017) S. cerevisiae Trm140 has two recognition modes for 3-methylcytidine modification of the anticodon loop of tRNA substrates. *RNA 23*, 406−419.
(30) Iwanami, Y., and Brown, G. M. (1968) Methylated bases of transfer ribonucleic acid from HeLa and L cells. *Arch. Biochem. Biophys. 124*, 472−482.
(31) Noma, A., Yi, S., Katoh, T., Takai, Y., Suzuki, T., and Suzuki, T. (2011) Actin-binding protein ABP140 is a methyltransferase for 3-methylcytidine at position 32 of tRNAs in Saccharomyces cerevisiae. *RNA 17*, 1111−1119.
(32) Olson, M. V., Page, G. S., Sentenac, A., Piper, P. W., Worthington, M., Weiss, R. B., and Hall, B. D. (1981) Only one of two closely related yeast suppressor tRNA genes contains an intervening sequence. *Nature 291*, 464−469.
(33) Liu, F., and He, C. (2017) A new modification for mammalian messenger RNA. *J. Biol. Chem. 292*, 14704−14705.
(34) Xu, L., Liu, X., Sheng, N., Oo, K. S., Liang, J., Chionh, Y. H., Xu, J., Ye, F., Gao, Y. G., Dedon, P. C., and Fu, X. Y. (2017) Three distinct 3-methylcytidine (m(3)C) methyltransferases modify tRNA and mRNA in mice and humans. *J. Biol. Chem. 292*, 14695−14703.
(35) McIntyre, W., Netzband, R., Bonenfant, G., Biegel, J. M., Miller, C., Fuchs, G., Henderson, E., Arra, M., Canki, M., Fabris, D., and Pager, C. T. (2018) Positive-sense RNA viruses reveal the complexity and dynamics of the cellular and viral epitranscriptomes during infection. *Nucleic Acids Res. 46*, 5776−5791.
(36) Chen, Z., Qi, M., Shen, B., Luo, G., Wu, Y., Li, J., Lu, Z., Zheng, Z., Dai, Q., and Wang, H. (2019) Transfer RNA demethylase ALKBH3 promotes cancer progression via induction of tRNA-derived small RNAs. *Nucleic Acids Res. 47*, 2533−2545.
(37) Ougland, R., Zhang, C. M., Liiv, A., Johansen, R. F., Seeberg, E., Hou, Y. M., Remme, J., and Falnes, P. O. (2004) AlkB restores the biological function of mRNA and tRNA inactivated by chemical methylation. *Mol. Cell 16*, 107−116.
(38) Ueda, Y., Ooshio, I., Fusamae, Y., Kitae, K., Kawaguchi, M., Jingushi, K., Hase, H., Harada, K., Hirata, K., and Tsujikawa, K. (2017) AlkB homolog 3-mediated tRNA demethylation promotes protein synthesis in cancer cells. *Sci. Rep. 7*, 42271.
(39) Brookes, P., and Lawley, P. D. (1962) The Methylation of Cytosine and Cytidine. *J. Chem. Soc.*, 1348−1351.
(40) Ogilvie, K. K., and Kader, H. A. (1983) Synthesis of 3, N4-Dimethylcytidine. *Nucleosides Nucleotides 2*, 345−350.
(41) McDowell, J. A., and Turner, D. H. (1996) Investigation of the structural basis for thermodynamic stabilities of tandem GU mismatches: solution structure of (rGAGGUCUC)2 by two-dimensional NMR and simulated annealing. *Biochemistry 35*, 14077−14089.

https://dx.doi.org/10.1021/acschembio.0c00735
ACS Chem. Biol. 2021, 16, 76−85

(42) Feldblum, E. S., and Arkin, I. T. (2014) Strength of a bifurcated H bond. *Proc. Natl. Acad. Sci. U. S. A. 111*, 4085−4090.
(43) Myers, J. C., Spiegelman, S., and Kacian, D. L. (1977) Synthesis of full-length DNA copies of avian myeloblastosis virus RNA in high yields. *Proc. Natl. Acad. Sci. U. S. A. 74*, 2840−2843.
(44) Motorin, Y., Muller, S., Behm-Ansmant, I., and Branlant, C. (2007) Identification of modified residues in RNAs by reverse transcription-based methods. *Methods Enzymol. 425*, 21−53.
(45) Skasko, M., Weiss, K. K., Reynolds, H. M., Jamburuthugoda, V., Lee, K., and Kim, B. (2005) Mechanistic differences in RNA-dependent DNA polymerization and fidelity between murine leukemia virus and HIV-1 reverse transcriptases. *J. Biol. Chem. 280*, 12190−12200.
(46) Potapov, V., Fu, X., Dai, N., Correa, I. R., Jr., Tanner, N. A., and Ong, J. L. (2018) Base modifications affecting RNA polymerase and reverse transcriptase fidelity. *Nucleic Acids Res. 46*, 5753−5763.
(47) Preston, B. D., Poiesz, B. J., and Loeb, L. A. (1988) Fidelity of HIV-1 reverse transcriptase. *Science 242*, 1168−1171.
(48) Cornell, W. D., Cieplak, P., Bayly, C. I., Gould, I. R., Merz, K. M., Ferguson, D. M., Spellmeyer, D. C., Fox, T., Caldwell, J. W., and Kollman, P. A. (1995) A Second Generation Force Field for the Simulation of Proteins, Nucleic Acids, and Organic Molecules. *J. Am. Chem. Soc. 117*, 5179−5197.
(49) Jakalian, A., Jack, D. B., and Bayly, C. I. (2002) Fast, efficient generation of high-quality atomic charges. AM1-BCC model: II. Parameterization and validation. *J. Comput. Chem. 23*, 1623−1641.
(50) Cornell, W. D., Cieplak, P., Bayly, C. I., and Kollman, P. A. (1993) Application of RESP charges to calculate conformational energies, hydrogen bond energies, and free energies of solvation. *J. Am. Chem. Soc. 115*, 9620−9631.
(51) Chen, A. A., and Garcia, A. E. (2013) High-resolution reversible folding of hyperstable RNA tetraloops using molecular dynamics simulations. *Proc. Natl. Acad. Sci. U. S. A. 110*, 16820−16825.
(52) Abraham, M. J., Murtola, T., Schulz, R., Páll, S., Smith, J. C., Hess, B., and Lindahl, E. (2015) GROMACS: High performance molecular simulations through multi-level parallelism from laptops to supercomputers. *SoftwareX 1−2*, 19−25.
(53) Bussi, G., Donadio, D., and Parrinello, M. (2007) Canonical sampling through velocity rescaling. *J. Chem. Phys. 126*, 014101.
(54) Berendsen, H. J. C., Postma, J. P. M., van Gunsteren, W. F., DiNola, A., and Haak, J. R. (1984) Molecular dynamics with coupling to an external bath. *J. Chem. Phys. 81*, 3684−3690.
(55) Darden, T., York, D., and Pedersen, L. (1993) Particle mesh Ewald: An N·log(N) method for Ewald sums in large systems. *J. Chem. Phys. 98*, 10089−10092.
(56) Jorgensen, W. L., Chandrasekhar, J., Madura, J. D., Impey, R. W., and Klein, M. L. (1983) Comparison of simple potential functions for simulating liquid water. *J. Chem. Phys. 79*, 926−935.
(57) Hess, B., Bekker, H., Berendsen, H. J. C., and Fraaije, J. G. E. M. (1997) LINCS: A linear constraint solver for molecular simulations. *J. Comput. Chem. 18*, 1463−1472.

https://dx.doi.org/10.1021/acschembio.0c00735
ACS Chem. Biol. 2021, 16, 76−85